EPJ E
Soft Matter and Biological Physics
EPJ.org
your physics journal

Eur. Phys. J. E (2012) **35**: 20 DOI 10.1140/epje/i2012-12020-3

Stress propagation in a concentrated colloidal suspension under shear

N.S. Martys, M. Khalil, W.L. George, D. Lootens and P. Hébraud

EDP SCIENCES
Società Italiana di Fisica
Springer

Eur. Phys. J. E (2012) **35**: 20
DOI 10.1140/epje/i2012-12020-3

THE EUROPEAN PHYSICAL JOURNAL E

Regular Article

Stress propagation in a concentrated colloidal suspension under shear

N.S. Martys[1], M. Khalil[2], W.L. George[1], D. Lootens[3], and P. Hébraud[2,a]

[1] National Institute of Standards and Technology, 100 Bureau Drive, Stop 8615, Gaithersburg, MD 20899-8615, USA
[2] IPCMS, CNRS, 23 rue du Loess, 67034 Strasbourg Cedex, France
[3] Sika Technology A.G., Tüffenwies 16, CH-8048 Zürich, Switzerland

Received 12 September 2011 and Received in final form 23 February 2012
Published online: 21 March 2012 – © EDP Sciences / Società Italiana di Fisica / Springer-Verlag 2012

Abstract. The stress propagation in a concentrated attractive colloidal suspension under shear is studied using numerical simulations. The spatial correlations of the intercolloidal stress field are studied and an inertia-like tensor is defined in order to characterize the anisotropic nature of the stress field. It is shown that the colloids remain in a liquid order, the intercolloidal stress is strongly anisotropic. A transition under flow is observed: during a transient regime at low deformation, the stress propagates along the compression direction of the shear, whereas at larger deformations, the stress is organized into layers parallel to the (flow, vorticity) plane.

When subject to shear, concentrated colloidal suspensions can organize into a wide variety of structures [1]. As a consequence, they do not behave as simple Newtonian fluids, and exhibit a rich phenomenology of macroscopic rheological behaviors. For instance, in the low Péclet number regime, the Brownian contribution to the stress increases slower than linearly with the shear rate, leading to shear thinning behavior [2]. Also, at low deformation rates, the viscosity of suspensions composed of attractive colloid particles decreases with the increase of deformation rate, due to the breakup of larger scale structures or alignment of the colloids parallel to the flow direction. On the contrary, at high deformation rates, the viscosity rapidly increases [3], or the suspension stops flowing [4–8]. It is thought that the formation of reversible clusters is responsible for this abrupt shear-thickening [10,11]. The jamming shear rate decreases when the rugosity of the particles increase, showing that contact stresses, including frictional stress, play a key role in the jamming process [6,9]. Understanding the relationship between the macroscopic rheological properties and the microstructure is a key challenge in the description of the flow of suspensions. Thus, many experiments have been devoted to the measurement of the positions of the colloids under shear, either in the direct space [12] or in the reciprocical space [13]. Simulations have also been used to measure the pair distribution function of strongly sheared suspensions [14–16]. One then searches to compute the macroscopic properties, using either continuous medium [17–19] or molecular type approaches [20]. Nevertheless, at high volume fractions and high shear rates, these approaches become increasingly difficult, as stress is dominated by the lubrication stress, localized between nearest colloids [10,21]. The contribution of the lubrication forces to the total stress is a function of the relative velocity of neighboring colloids. Moreover, the stress is extremely heterogeneous spatially. The situation is analogous to the case of granular suspensions [22], for which stress propagates along force chains that cannot be deduced from the grains positions knowledge, as the force at contacts is a friction and depends on the previous history of the grains.

In this article, we simulate the flow of a concentrated colloidal suspension and show that, although the colloids exhibit a liquid ordering, the intercolloidal stress is strongly anisotropic and heteregeneous. The colloids are chosen to be highly attractive so that the suspension aggregates at rest. As a consequence, "non-zero stress", as defned by stress growth experiments, is necessary to induce the flow of the suspension: it possesses an apparent yield stress [23]. We have shown in a previous study [24] that this yield stress originates not only from stress accumulated between pairs of colloids pulled apart by the flow but from stress accumulation between pairs of colloids aligned along the compression direction of the flow. When the suspension is sheared at an intermediate shear rate, the interactions between colloids are a combination of hydrodynamics and interaction forces. We develop a novel way of describing the microscopic stress field under flow and introduce an inertia-like tensor to describe its anisotropic nature. By comparing the statistical properties of the suspension density and of the intercolloidal stress field at different stages of the flow, we show that

[a] e-mail: pascal.hebraud@ipcms.unistra.fr

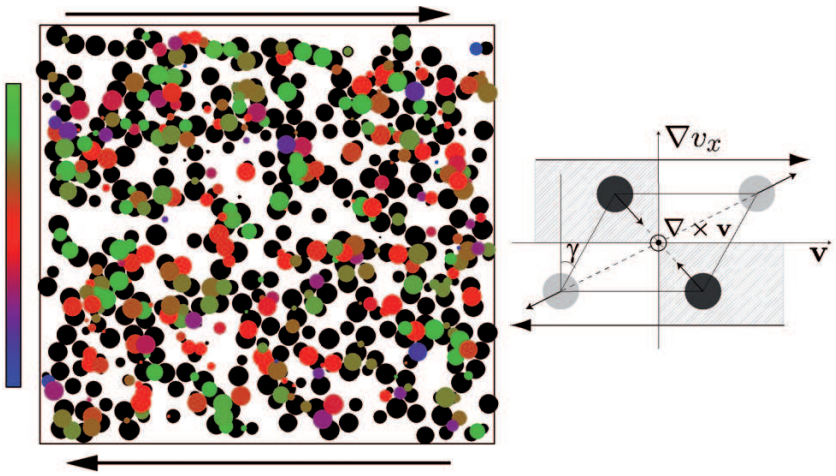

Fig. 1. (Colour on-line) Illustration of the stress field construction. The system has been strained by a value $\gamma = 0.067$. Real colloids whose center lies in a $(\mathbf{v}, \nabla v_x)$ slice of thickness equal to the colloids diameter are represented in black. Stress spheres belonging to the same slice are represented in color. The color code for the absolute value of the tangential stress supported by these spheres is given by the side bar with green representing the greatest stress magnitude. In both cases, the particle sizes correspond to the size of their intersection with the middle plane of the slice. Inset: definition of the compression quadrant of the shear deformation: dark grey particles are pushed together by the deformation. On the opposite, light grey particles are pulled apart.

concentrated colloidal suspensions possessing similar pair distribution functions may exhibit very different stress propagation mechanisms. We show that, as flow proceeds, the stress propagation evolves from propagation along the compression quadrant of the shear deformation (fig. 1 inset) towards propagation in a plane approximately parallel to the flow direction.

We perform numerical simulation of the flow and use the Dissipative Particle Dynamics [25] (DPD) technique to model the flow of such suspension. DPD has been shown to agree with Stokesian Dynamics simulations to describe the flow properies of highly concentrated suspensions [25–27]. This approach can roughly be thought of as a Lagrangian formulation of Navier Stokes with thermal fluctuations [28]. The DPD simulation is similar in structure to molecular dynamics simulation but, instead of modeling all the molecular properties of the system, the motion of mesoscopic DPD particles that represent a coarse-grained fluid are considered [25,29]. The DPD particles are subjected to conservative, dissipative and random forces [30]

$$\mathbf{F}_{ij} = \mathbf{F}^C_{ij} + \mathbf{F}^D_{ij} + \mathbf{F}^R_{ij}. \tag{1}$$

The conservative force is a soft repulsive radial force that decreases linearly with the center-to-center distance, $|\mathbf{r}_i - \mathbf{r}_j|$, between the two DPD particles i and j, and whose amplitude is chosen so that the compressibility of the DPD fluid matches that of water. The dissipative force is proportional to the difference of velocities between DPD particles i and j, $\mathbf{v}_i - \mathbf{v}_j$, and acts to slow down their relative motion, producing a viscous effect. Lastly, a random force is added that controls the temperature of the system. The dissipative and random forces control the viscosity of the fluid and, to maintain a well-defined temperature, are related by the fluctuation-dissipation theorem [31]. In contrast to the individual DPD particles, a colloid is then defined as an assembly of constrained DPD particles so that they form a rigid body.

The colloids are submitted to two additional forces. The first one derives from an interaction potential. We use a Derjaguin-type approximation of the Lennard-Jones interactions [32] between colloid spheres A and B at short distances. This potential scales as the sum of a hard-sphere repulsion term, A_{HS}/s^7_{AB} and a van der Waals potential, H/s_{AB}, where A_{HS} and H are constants related to the hard-sphere potential and to the Hamaker constant respectively, and s_{AB} is the distance between the two colloids surfaces. The second additional force is a lubrication force, explicitly computed from the relative surface motion of the colloids [25, 33, 35]. Both forces are modified by a smoothing function so that a cut-off distance of the order of the colloids radius is introduced, that prevents the divergence of the energy. Details of the computation of these forces are given in [24, 25].

The colloidal particles are attractive, and in the absence of flow, the suspension evolves to form a colloidal gel. We follow a well-defined preparation protocol of the suspension. It is prepared by randomly placing the spheres in a cubic cell, with small overlaps being possible. Then, a repulsive force is applied between spheres if they overlap. Once all the spheres no longer overlap, the system is allowed to equilibrate under the action of Brownian and hydrodynamic forces. When a stable radial distribution function is obtained, the van der Waals and lubrication forces are introduced by turning them on slowly enough so that the additional kinetic energy produced in the system, because two spheres are too close to each other, is allowed to dissipate. We choose the end of the introduction of the van der Waals and the lubrication forces as the initial time of the system. Then, for a given waiting time,

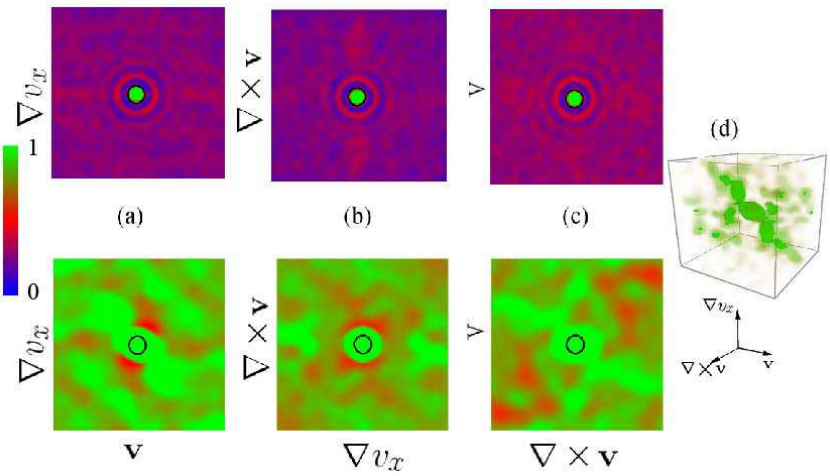

Fig. 2. (Colour on-line) Correlation field of the colloids positions, C_ρ, (upper row) and of the intercolloidal tangential stress, C_σ, (bottom row) after a deformation $\gamma = 0.067$. Slices of this correlation field along each plane $(\mathbf{v}, \nabla v_x)$ (column (a)), $(\nabla v_x, \nabla \times \mathbf{v})$ (column (b)) and $(\nabla \times \mathbf{v}, \mathbf{v})$ (column (c)) are given. The color code is given by the side bar. The three-dimensional stress surface is plotted in (d). Here the translucency is adjusted to highlight the largest values of stress correlation.

the suspension is allowed to evolve towards a flocculated colloidal gel. After this aging time, the shear is applied to the sample.

The colloid's radius is the only length scale explicitly included in the description of the suspension. The parameters chosen for the simulation correspond to spherical alumina colloids of approximately 100 nm diameter. The interaction potential between two colloids exhibits a minimum of $25k_\mathrm{B}T$ at a distance of 6 nm between the surfaces. The time integration scheme for the DPD particles and the colloids is based on a velocity-Verlet algorithm [25,36]. We follow the motion of 9616 colloids whose volume fraction is 50%, under a deformation rate $\dot{\gamma} = 2100\ \mathrm{s}^{-1}$, and for deformations ranging from 0 to 4. During flow, our system is fully characterized by two non-dimensional numbers: the Péclet number and a second number which gives the ratio of the hydrodynamic force *vs.* the maximum force of interaction. First, the Péclet number, $Pe = \frac{4\pi\mu\dot{\gamma}a^3}{k_B T}$ is equal to 24 so that in this flow regime advection dominates over diffusion. In this study, the deformation rate was chosen so that the interactions between colloids remain important, and the system is not dominated by pure hydrodynamic interactions. A second non-dimensional number may be built, $6\pi\mu a^2\dot{\gamma}/F_\mathrm{max}$, where a is the radius of the colloids, F_max the maximum attractive force between colloids and μ is the fluid viscosity. Its value is 0.044 in this study indicating that the interparticle interactions is still dominant over hydrodynamic forces. Further, the values of non-dimensional parameters chosen in this study also correspond to suspensions of larger size, such as 1 μm colloids under a shear rate equal to 2.1 s^{-1}, with a minimum interaction potential equal to $2.5k_\mathrm{B}T$.

In order to describe the transmission of stress throughout the suspension we need to first identify neighboring colloids in close contact. In our simulations, it was observed that whatever the deformation value, the pair distribution function exhibits a well-defined peak at contact [24]. We identified the colloids in contact as those whose surface-to-surface distance is smaller than the width of the first peak of the pair distribution function. Given the set of spheres in contact, we construct a dual space of spheres that are placed at the midpoint between the centers of neighboring colloids in contact (fig. 1). Then each dual sphere is assigned the stress in the continuous medium at the contact point. When defined over length scales shorter than colloid-colloid interactions, the microscopic stress tensor is ambiguously defined [37]: it is necessary to define pairs of colloids that do contribute to the stress onto the small surface considered. Irving and Kirkwood chose to consider only pairs of colloids whose center-to-center segment crosses the considered small surface [38], whatever their distance. In our case, we are interested in the value of the stress contact points between pairs of colloids. Both the lubrication and the potential part of the stress diverges when colloids come closer, and the stress is dominated by the two colloids in contact. Hence, we only consider the contribution of the stress arising from colloids with pair-wise contacts. This dual space is chosen as it emphasizes the role of the intercolloidal stress, and allows for computation of the stress correlation, from colloid to colloid, throughout the suspension. The minimum length of stress propagation is equal to the diameter of the colloids, so we chose this length as the diameter of the stress spheres. Although this choice is in part arbitrary, we feel that it is representative of the mechanism of stress propagation. It brings out the continuity of the stress (two diametrically opposite points of contact lead to two touching stress spheres) without reducing the continuity of the structure. We obtain the stress field between colloids in pair-wise contact in the suspension, $\sigma_{xy}(\mathbf{r})$. Due to the presence of a large number of contacts, the volume fraction of the stress spheres is observed to be higher than the volume fraction of the colloids, and they may overlap. In that case, we chose to add the stresses in the overlapping

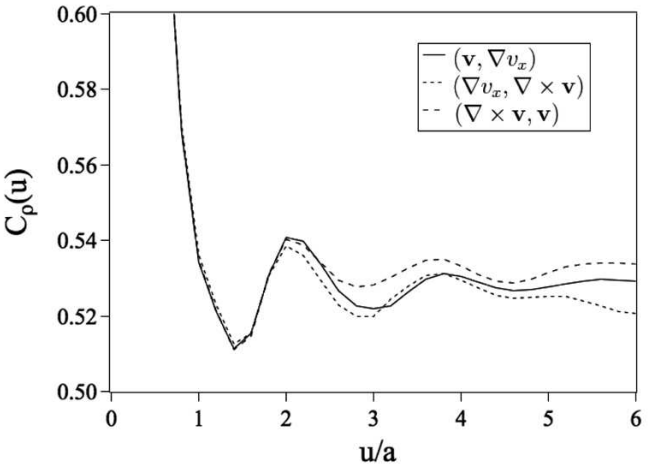

Fig. 3. Radial correlation of the colloids positions, in each plane $(\mathbf{v}, \nabla v_x)$, $(\nabla v_x, \nabla \times \mathbf{v})$ and $(\nabla \times \mathbf{v}, \mathbf{v})$ for a deformation $\gamma = 0.067$.

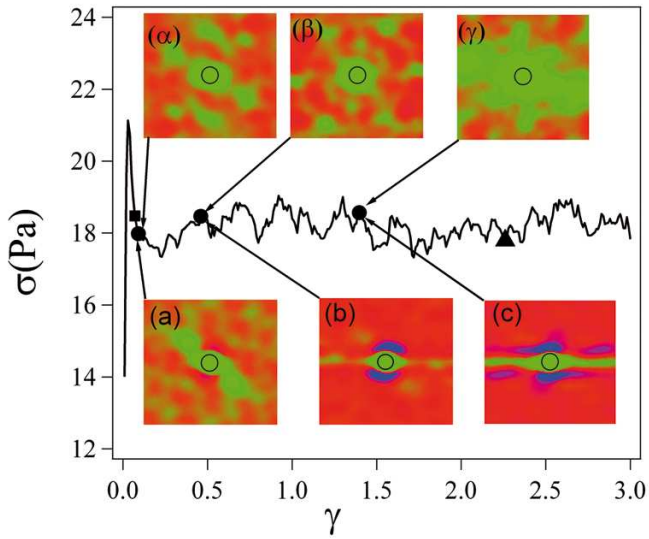

Fig. 4. (Colour on-line) Shear stress as a function of the strain. Stress correlation surfaces C_σ along the $(\nabla \times \mathbf{v}, \mathbf{v})$ plane (upper images) and along the $(\mathbf{v}, \nabla v_x)$ plane (lower images) are represented, for three different deformation values: $\gamma = 0.09$, $\gamma = 0.46$ and $\gamma = 1.4$. The square and the triangle correspond to the stress/deformation values of the correlations plotted in fig. 2 and fig. 6, respectively. The color code for the absolute value of the tangential stress supported by these spheres is given by the side bar of Fig. 2.

region. We compute the spatial correlation of this stress field

$$C_\sigma(\mathbf{u}) = \frac{\langle \sigma_{xy}(\mathbf{r})\sigma_{xy}(\mathbf{r}+\mathbf{u})\rangle_\mathbf{r}}{\langle \sigma_{xy}(\mathbf{r})^2\rangle_\mathbf{r}}, \tag{2}$$

where $\mathbf{u}$ is a translation vector and $\langle ... \rangle_\mathbf{r}$ is the average over space. To compare the stress field properties with the colloids organization under flow, we also define the colloids position correlation, $C_\rho(\mathbf{u})$, where σ_{xy} is replaced by the local density, ρ, whose value is 1 inside a colloid and 0 outside. After a small deformation value, the colloids exhibit liquid ordering (fig. 3), whereas the stress correlation is anisotropic (fig. 2).

Indeed, whatever the position of the translation vector $\mathbf{u}$ relative to the flow direction, the correlation pattern of the colloids positions exhibit a liquid pattern, characterized by a series of circular fringes of decreasing amplitudes (fig. 2a,b,c upper row) [39]. The stress correlation possesses several remarkable features (fig. 2a,b,c lower row):

- it is mainly oriented along the compression direction of the shear flow, in the $(\mathbf{v}, \nabla v_x)$ plane,
- the stress possesses a long-range correlation length (larger than the stress sphere size), in all the spatial directions.

The first observation is in agreement with our previous study of a similar system at the onset of flow [24], where we showed that, at small deformations and for concentrated suspensions, the stress needed to make the suspension flow is stored in intercolloidal contacts oriented along the compression direction of the shear. Our analysis here shows moreover that long-range correlation of the stress is observed in the compression quadrant (fig. 4, square symbol).

Then, as flow proceeds, the excess of correlation in the compression quadrant is lost and anticorrelation of the stress is observed in the ∇v_x direction, at a distance $2r$ (fig. 4, image (b)). This anticorrelation progressively develops and we reach a stationary regime in which the stress correlation is highly anisotropic, and most of the correlation is observed along the $(\mathbf{v}, \nabla \times \mathbf{v})$ plane (fig. 4, image (c)). This progressive buildup of anisotropy of the stress propagation in the suspensions may be characterized by considering the correlation volume as a solid body weighted by the correlation value of the stress tensor. We define the inertia tensor of the stress correlation field

$$\mathbb{J}_\sigma = \iiint C_\sigma(\mathbf{u}) \left(u^2\mathbb{I} - \mathbf{u}\otimes\mathbf{u}\right) \mathrm{d}^3\mathbf{u}. \tag{3}$$

We then diagonalize this tensor and define $\lambda_1 \leq \lambda_2 \leq \lambda_3$ its three eigenvalues and $\mathbf{u}_1$, $\mathbf{u}_2$ and $\mathbf{u}_3$ the corresponding eigenvectors. We define $\epsilon = \lambda_3/\lambda_1$ and $\rho = \lambda_3/\lambda_2$. For a perfect disk shape, we would have $\epsilon = 2$ and $\rho = 1$. At initial deformations, the shape of the stress correlation is isotropic and $\lambda_1 \simeq \lambda_2 \simeq \lambda_3$, so that $\epsilon \simeq 1$ and $\rho \simeq 1$. Then, when deformation proceeds, the disk shape develops: ρ fluctuates around 1 and the anisotropy factor ϵ progressively increases (fig. 5(a)). At the highest deformation reached by our simulations, the asymptotic value of ϵ is not yet reached. Conversely, the stress correlation volume becomes anisotropic and rapidly orientates parallel to the flow: the angle ϕ of the eigenvector of lowest eigenvalue fluctuates very rapidly at short deformations and then, after a characteristic deformation $\gamma_c \simeq 0.8$, tends towards 0 (fig. 5(b)). The propagation of stress no longer occurs in the compression quadrant of the deformation, but in a plane parallel to the flow direction, corresponding to $\phi = 0$. This stress propagation cannot be explained by the underlying organization of the colloids, as no layering (or

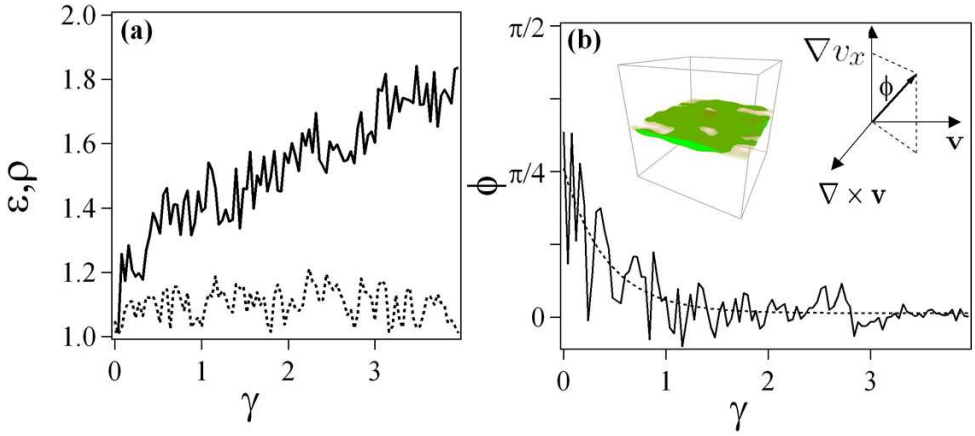

Fig. 5. (a) Evolution of the ratio of the eigenvalues of the inertia-like tensor (defined by 3) of the stress correlation volume, considered as a weighted solid body (ϵ: solid line, ρ: dashed line). (b) Angle ϕ of the main axis of rotation of the stress correlation volume as a function of the deformation (solid line). The dashed line is an exponential fit to the data, $\phi = \phi_0 e^{-\gamma/\gamma_c}$. A representative 3-D surface of the stress correlation field (at $\gamma = 2.28$) and the definition of the Euler angle ϕ are given in the inset.

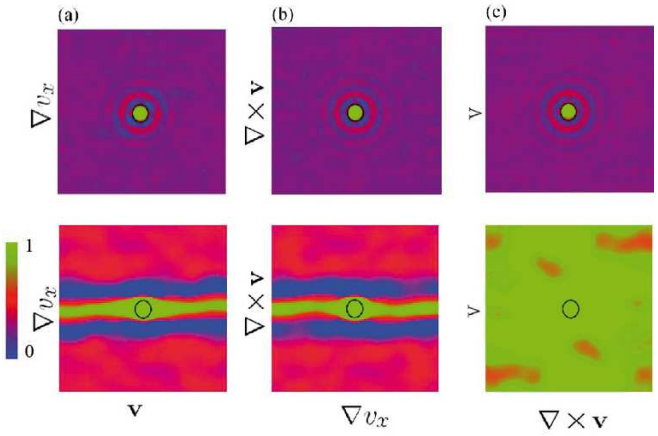

Fig. 6. (Colour on-line) Correlation field of the colloids positions (upper row) and of the intercolloidal tangential stress (bottom row) after a deformation $\gamma = 2.28$. Slices of this correlation field along each plane $(\mathbf{v}, \nabla v_x)$ (column (a)), $(\nabla v_x, \nabla \times \mathbf{v})$ (column (b)) and $(\nabla \times \mathbf{v}, \mathbf{v})$ (column (c)) are given.

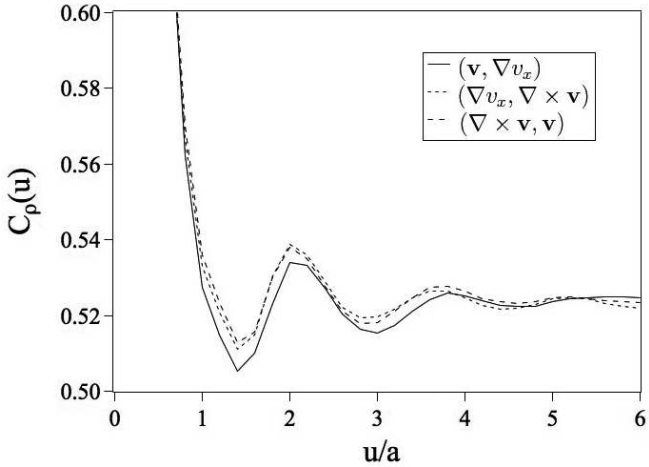

Fig. 7. Radial correlation of the colloids positions, in each plane $(\mathbf{v}, \nabla v_x)$, $(\nabla v_x, \nabla \times \mathbf{v})$ and $(\nabla \times \mathbf{v}, \mathbf{v})$ for a deformation $\gamma = 2.28$.

at best very weak layering) is exhibited in their organization (fig. 6 upper row, fig. 7 and fig. 8(a)). It can neither be due solely to the organization of the contact spheres (fig. 8(a)). Their spatial organization is more heterogeneous than the colloids themselves and regions of characteristic dimension of the order of 2–3 colloids do exist in which no contact is observed (fig. 8(b)). Nevertheless, these regions are not oriented along the flow and do not exhibit any spatial heterogeneity. Thus, the weighting of the contact network by local stresses is responsible for the excess of stress correlation along a plane normal to the gradient velocity of the flow.

Looking closely at the stress correlation field in the $(\mathbf{v}, \nabla \times \mathbf{v})$ plane, we observe that the stress correlation does not exhibit a monotonic decay along this plane, but possesses several maxima. Correlation maxima at distances much larger than a single stress sphere diameter are observed (fig. 4, α to γ). This fine structure exhibits two striking properties: the stress correlation maxima sometimes present a transient 6-fold symmetry, and they very rapidly evolve under flow over deformations smaller than a strain of 0.01. These observations are consistent with the experimental observation of rapid stress fluctuations [5,7], and show that fragile stress paths do form in colloidal suspensions [40]. These paths are not oriented along the compression direction of the deformation, but along a plane parallel to the flow direction. Moreover, albeit the colloids do not crystallize under flow (fig. 6(a) to (c)), these stress paths exhibit a transient hexagonal symmetry. Thus, the properties of stress propagation are not reflective of the organization of the colloids, but of the underlying network of neighboring colloids that support stress propagation.

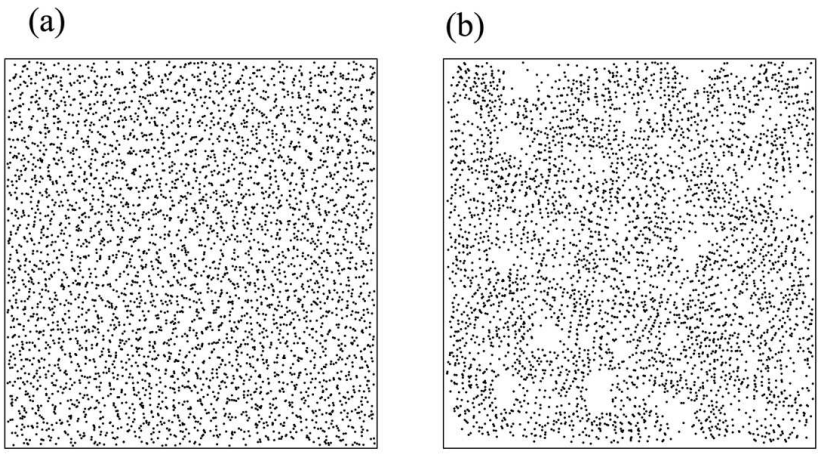

Fig. 8. Centers of colloids (a), respectively, of stress spheres (b), in a $(\mathbf{v}, \nabla v_x)$ slice of thickness 10, respectively, 2, colloid diameters, after the deformation $\gamma = 2.28$.

This network is strongly anisotropic and it very rapidly fluctuates under flow.

To understand the rheological properties of a concentrated colloidal suspension, it is necessary to make a link between the microscopic behavior and the macroscopic properties which can depend on the colloidal interactions. At small strains there was a significant amount of stress transmitted in compression (fig. 2(a)). This is a consequence of the microstructure reorganizing from the initial isotropic colloidal network to one associated with the dynamic equilibrium of an anisotropic flow at later stages [24]. At the small strains there is an accompanying sharp rise in stress (fig. 4) which is often seen in stress growth curves. The peak of the stress growth is sometimes associated with the yield stress of the fluid. However, this yield stress is a function of shear rate and appears to go to zero with decreasing shear rate due to thermal fluctuations. At higher strains, scattering experiments [13] and numerical simulations [41,42] of hard-spheres suspensions do not show order under flow. On the opposite, respulsive particles can present flow ordering [34]. Here, by studying a system of strongly aggregated particles under flow, we have shown that, although particles do not exhibit layering (or very little layering) along the flow, the stress pattern is strongly anisotropic. In this regime of small interparticle distances, the stresses between adjacent colloids dominates the rheological response. We have chosen to emphasize the intercolloidal stress field, but other complementary fields may be needed to more fully describe the flow. Examples could be the complete stress field (not only between pairs of colloids in contact), or the velocity field of the colloids which may be experimentally easier to measure.

We would like to gratefully acknowledge support from the Virtual Cement and Concrete testing Laboratory consortium (VCCTL). The flow simulations were performed under award SMD-05-A-0129, "Modeling the Rheological Properties of Suspensions: Applications to Cement Based Materials" for NASA's National Leadership Computing System Initiative on the "Columbia" supercomputer at the NASA Ames Research Center. This research used resources of the Argonne Leadership Computing Facility at Argonne National Laboratory, which is supported by the Office of Science of the U.S. Department of Energy under contract DE-AC02-06CH11357.

References

1. P. Varadan, M.J. Solomon, J. Rheol. **47**, 943 (2003).
2. X. Cheng, J.H. McCoy, J.N. Israelachvili, I. Cohen, Science **333**, 1276 (2011).
3. N.J. Wagner, J.F. Brady, Phys. Today, October issue, 27 (2009).
4. B.J. Maranzano, N.J. Wagner, J. Chem. Phys. **117**, 10291 (2002).
5. D. Lootens, H. Van Damme, P. Hébraud, Phys. Rev. Lett. **90**, 178301 (2003).
6. D. Lootens, H. van Damme, Y. Hémar, P. Hébraud, Phys. Rev. Lett. **95**, 268302 (2005).
7. M.D. Haw, Phys. Rev. Lett. **92**, 185506 (2004).
8. D. Lootens, P. Hébraud, É. Lécolier, H. van Damme, Oil Gas Sci. Technol. **59**, 31 (2004).
9. E. Brown, N.A. Forman, C.S. Orellana, H. Zhang, B.W. Maynor, D.E. Betts, J.M. DeSimone, H.M. Jaeger, Nat. Mater. **9**, 220 (2010).
10. R.S. Farr, J.R. Melrose, R.C. Ball, Phys. Rev. E **55**, 7203 (1997).
11. F. Ianni, D. Lasne, R. Sarcia, P. Hébraud, Phys. Rev. E **74**, 011401 (2006).
12. P. Schall, D.A. Weitz, F. Spaepen, Science **318**, 1895 (2007).
13. B.J. Maranzano, N.J. Wagner, J. Chem. Phys. **117**, 10291 (2002).
14. J.F. Brady, J.F. Morris, J. Fluid Mech. **348**, 103 (1997).
15. A. Sierou, J.F. Brady, J. Rheol. **46**, 1031 (2002).
16. J. Bergenholtz, J.F. Brady, M. Vicic, J. Fluid Mech. **456**, 239 (2002).
17. D.A. Drew, Annu. Rev. Fluid Mech. **15**, 261 (1983).
18. R.I. Nigmatulin, *Dynamics of Multiphase Media* (Hemisphere, New York, 1991).

19. D. Lhuillier, Eur. J. Mech. B **11**, 649 (1992).
20. J.K.G. Dhont, *An Introduction to the Dynamics of Colloids, Elsevier Series in Interface Science* (Elsevier, 1996).
21. L.E. Silbert, R.S. Farr, J.R. Melrose, R.C. Ball, J. Chem. Phys. **111**, 4780 (1999).
22. M.E. Cates, J.P. Wittmer, J.-Ph. Bouchaud, P. Claudin, Phys. Rev. Lett. **81**, 1841 (1998).
23. R.G. Larson, *The Structure and Rheology of Complex Fluids* (Oxford University Press, New York, 1999).
24. N.S. Martys, D. Lootens, W. George, P. Hébraud, Phys. Rev. E **80**, 031401 (2009).
25. N.S. Martys, J. Rheol. **49**, 401 (2005).
26. W. Pan, B. Caswell, G.E. Karniadakis, Langmuir **26**, 133 (2009).
27. D.R. Foss, J.F. Brady, J. Fluid Mech. **407**, 167 (2000).
28. P. Español, M. Revenga, Phys. Rev. E **67**, 026705 (2003).
29. P.J. Hoogerbrugge, J.M.V.A. Koelman, Europhys. Lett. **19**, 155 (1992).
30. R.D. Groot, P.B. Warren, J. Chem. Phys. **107**, 4423 (1997).
31. P. Español, P. Warren, Europhys. Lett. **30**, 191 (1995).
32. J.N. Israelachvili, *Intermolecular and Surface Forces* (Academic Press, 1992).
33. S. Kim, S.J. Karrila *Microhydrodynamics* (Butterwort-Heinemann, 1991).
34. L.B. Chenb, C.F. Zukoski, B.J Ackerson, H.J.M. Hanley, G.C. Straty, J. Barker, C.J. Glinka, Phys. Rev. Lett. **69**, 688 (1992).
35. E. Boek, P.V. Coveney, H.N. Lekkerkerker, P. Van der Schoot, Phys. Rev. E **55**, 3124 (1997).
36. N.S. Martys, R.D. Mountain, Phys. Rev. E **59**, 3733 (1999).
37. F. Varnik, J. Baschnagel, K. Binder, J. Chem. Phys. **113**, 4444 (2000).
38. J.H. Irving, J.G. Kirkwood, J. Chem. Phys. **18**, 817 (1950).
39. J.-P. Hansen, I.R. McDonald, *Theory of simple liquids* (Academic Press, 2006).
40. R. Sarcia, P. Hébraud, Phys. Rev. E **72**, 011402 (2005).
41. A. Sierou, J.F. Brady, J. Rheol. **46**, 1031 (2002).
42. J.F. Brady, J.F. Morris, J. Fluid Mech. **348**, 103 (1997).